Encapsulation of ammonium molybdophosphate and zirconium phosphate in alginate matrix for the sorption of rubidium(I)

Pawel Krys, Flaviano Testa, Andrzej Trochimczuk, Christian Pin, Jean-Marie Taulemesse, Thierry Vincent, Eric Guibal

Encapsulation of ammonium molybdophosphate and zirconium phosphate in alginate matrix for the sorption of rubidium(I)

Pawel Krys [a,b], Flaviano Testa [a,c], Andrzej Trochimczuk [b], Christian Pin [d], Jean-Marie Taulemesse [a], Thierry Vincent [a], Eric Guibal [a,*]

[a] Ecole des mines d'Alès, Centre des Matériaux des Mines d'Alès, F-30319 Alès cedex, France
[b] Wrocław University of Technology, Faculty of Chemistry, P-50-370 Wrocław, Poland
[c] Università della Calabria, Dipartimento di Ingegneria Chimica e dei Materiali, Cubo 44A, Via Pietro Bucci, I-87030 Arcavacata di Rende, Italy
[d] Département de Géologie, CNRS & Université Blaise Pascal, CNRS, 5 rue Kessler, F-63038 Clermont-Ferrand cedex, France

A B S T R A C T

Ammonium molybdophosphate and Phozir (alone or in combination) have been encapsulated in alginate beads for the synthesis of rubidium sorbents. SEM and SEM–EDX analyses confirm the homogeneity of the sorbents in terms of composition and metal binding. AMP sorbent is less sensitive to pH than Phozir, and optimum pH is close to pH 3 for the binding of Rb(I). The Langmuir equation fitted well sorption iso-therms and the maximum sorption capacities were in the range 0.65–0.74 mmol Rb g^{-1}. The resistance to intraparticle diffusion contributes to control uptake kinetics (effect of particle size) though the presence of solid inorganic particles reduces the impact of drying alginate capsules (preventing the collapse of the porous structure during the drying step). Breakthrough curves demonstrate the potential of these sor-bents for the dynamic sorption of Rb(I) while using ammonium chloride (combined to nitric acid) allows recovering Rb(I) from loaded sorbents.

Keywords:
Rubidium
Alginate
Ammonium phosphomolybdate
Zirconium phosphate
pH effect
Sorption isotherms
SEM–EDX analysis
Breakthrough curves
Desorption

1. Introduction

The rarefaction of mineral resources due to the extensive exploitation of readily available sources and the increasing demand on strategic and precious metals (for the design of high materials) may explain the development of new processes for the recovery of these metals from dilute effluents, low ore, or from secondary sources (including the recycling of spent materials). Among these strategic metals, rare earth metals, some alkaline and alkaline earth metals are important targets. Rubidium and cesium are part of these metals that retained great attention during the last decade. This interest is also justified by the presence of dangerous radioisotopes of Cs in the effluents generated by the nuclear industry. Their high transport properties in water, soils, plants and human body require strict control when these metals are present as radionuclides because of their harmful effect on human beings. The recovery of these elements at trace levels is also an important challenge for analytical sciences: the pre-concentration of the trace metals and their separation from complex matrices (issued for example from the mineralization of soils and/or organic materials or from ore acid decomposition) [1].

Depending on the range of concentration and on the composition of effluents, several processes may be used for their extraction or removal including solvent extraction (high concentrations) [2], membranes and emulsion membranes (intermediate concentrations) [3,4], sorption on resins or impregnated resins (low concentration and simple effluents) [5–7]. However, in the case of dilute effluents and/or effluents containing high salinity (sea water, brines, and effluents from nuclear industry) the competition of cations from salt charge may drastically reduce the efficiency of these processes. Inorganic ion-exchange materials offer an interesting alternative since they have a great selectivity for these elements that allows their extraction from high ionic strength solutions (including sea water) [8]. A great diversity of mineral sorbents can be used for the recovery of cesium and/or rubidium: insoluble metal hexacyanoferrate (including Prussian blue [9–12]) [13–19], titanium dioxide [9–12], ammonium molybdophosphate [20–27], hydrogen (or sodium) zirconium phosphate [28–35], or titanium phosphate [36]. Their crystalline arrangement is responsible for the specific ion exchange of intercalated ions with target metal ions (even when the concentration of competitor ions is much larger than the concentration of target metals) [37,38]. The major

E-mail address: eric.guibal@mines-ales.fr (E. Guibal).

drawback of these materials for practical applications is due to their microcrystalline nature and their occurrence as fine-grained powders: the recovery of the sorbent (solid/liquid separation) in batch system or the hydrodynamic properties of fixed bed systems are then limiting criteria (pressure head loss, column blockage, sluggish flow rates, etc.). These problems may be circumvented by (a) immobilizing the inorganic ion-exchangers on oxide supports [39], such as silica [13,20,40–42], alumina [20,43] or (b) encapsulating these materials in synthetic polymers [18,21,25,32,44–47], or biopolymers [22,26,27,48]. The challenge then consists in managing simultaneously the confinement of the reactive mineral sorbents and the mass transfer properties (kinetics and accessibility to reactive sites).

In this study, two mineral sorbents, ammonium molybdophosphate (AMP) and hydrogen zirconium phosphate (Phozir), have been encapsulated (alone or in combination) in a biopolymer matrix made of alginate. Alginate is a biopolymer extracted from algal biomass, constituted by guluronic and mannuronic acid moieties (i.e., carboxylic groups held on pyranose groups). Alginate is able to bind metal cations through interactions with carboxylate groups (at pH above the pK_as of carboxylic acids; i.e., 3.35 and 3.65), especially with divalent cations. These interactions may be used for the ionotropic gelation of alginate: carboxylate groups of different polymer chains react with divalent cations (more specifically Ca(II)) to form the gel network (egg-box model) [49]. This gelation process is typically used for the encapsulation of enzymes, bacteria, drugs and even for the synthesis of new impregnated resins (immobilization of extractants [50], or ionic liquids [51]). The calcium-gelation process has been applied in the present study for the encapsulation of AMP and Phozir for designing Rb(I) sorbent.

The first part of the study describes the characterization of encapsulated materials before and after Rb(I) sorption using SEM and SEM–EDX analysis. In the second part the sorption properties are evaluated in batch systems (pH effect, sorption isotherms and uptake kinetics). Kinetic profiles have been compared for the different materials with a special attention to the state of composite capsules: wet beads, dried beads and freeze-dried beads in order to evaluate the restrictions to mass transfer induced by the drying procedure. Finally, the last part describes the sorption and desorption behavior of Rb(I) in dynamic systems (i.e., fixed-bed columns).

2. Materials and methods

2.1. Materials

Alginic acid was supplied by Acros Organics. Ammonium molybdophosphate hydrate (AMP) was obtained from Bio-Rad and Alpha Aesar. Zirconium phosphate (Phozir, $Zr[HPO_4]_2$) Calcium chloride hexahydrate were supplied by Riedel-de-Haen. Rubidium chloride was obtained from Chim-Lab. Other reagents were supplied by Sigma–Aldrich. All products are reagent grade.

2.2. Encapsulation process

Basically, the method consists in four steps: (a) the mixing of the encapsulating solution (i.e., alginate) with the mineral sorbent (i.e., Phozir, or AMP, or a blend of Phozir + AMP); (b) the extrusion of the resulting slurry through a thin nozzle (internal diameter 0.8 mm); (c) the gelation of the composite biopolymer/mineral drops into an agitated acidic calcium chloride solution (2% w/w calcium chloride hexahydrate, 0.02 M HCl); and (d) the rinsing of the beads with 0.01 M HCl.

The composition of the mixed alginate/mineral suspension was set at 360 g of alginate solution (at 2% w/w) and 40 g of an aqueous suspension of mineral sorbent (20 g of water plus 20 g of Phozir, or 20 g of AMP, or a mixture of 10 g of Phozir + 10 g of AMP).

In the case of Phozir encapsulation, a strong agitation proved to be necessary in order to disrupt the flocs that formed after the addition of the mineral sorbent. Besides this, during the extrusion of the viscous suspension, the drops falling down to the gelling solution did not form spherical particles, but ellipsoidal ones, whatever the depth of fall (which usually represents a critical parameter for the shaping of gel beads). In order to achieve the formation of spherical particles, the surface of the gelling solution was covered by a thin layer (i.e., 10 mm) of paraffin oil (density: 0.83). This oil layer contributed to give to the drops of alginate/mineral suspension the conditions (relaxation time, density, and viscosity) appropriate for getting the spherical shape before penetrating by gravity into the gelling medium. These specific conditions were not necessary when using AMP or Phozir in combination with AMP.

The extrusion was operated in most cases using a concentric double nozzle to prepare small size beads having a size ranging between 0.75 and 1 mm by the end of the process (including final drying). An airflow at the basis of the extrusion nozzle allowed sizing the beads. In the absence of such airflow, coarser beads formed before falling into the gelling solution (in the range 1.4–1.8 mm; DBL or WBL: Dried – D –, or Wet – W – Beads of Large size).

The beads were left in the gelling medium overnight before being rinsed three times with 0.01 M HCl. Wet beads (WB) were stored in 0.01 M HCl solutions, while dried beads were prepared by air-drying (in an oven, DB) or by freeze-drying (FD).

2.3. Material characterization

The morphology and the elemental distribution of mineral sorbents and Rb element in the composite materials were determined with a Scanning Electron Microscope coupled with an Energy Dispersive X-ray analysis system (SEM–EDX). These data were obtained by using an Environmental Scanning Electron Microscope (ESEM) Quanta FEG 200, equipped with an OXFORD Inca 350 Energy Dispersive X-ray microanalysis (EDX) system. The SEM observations were performed on the cross-section of the composite materials (obtained by cutting with a thin-slice cutter under a binocular microscope). Using environmental SEM allowed the direct observations of materials, without prior metallization of the samples. The topography of the samples was observed using secondary electrons while the backscattered electrons were used for the identification and localization of heavy metals at the surface of the materials (by phase contrast). SEM–EDX allowed to determine the distribution of elements on the cross-section by using mapping facilities and semi-quantitative analysis of the target metal Rb and that of the major components of the mineral sorbents; i.e., P, Zr and Mo.

2.4. Sorption experiments

The sorption experiments were performed in batch for the study of pH effect, sorption isotherms and uptake kinetics; breakthrough curves were also performed for the evaluation of sorption performances in the dynamic mode (fixed bed column).

For the study of pH effect 20 mL of 100 mg L^{-1} Rb(I) solutions at different pHs (between 1 and 6) were mixed with 50 mg of sorbent (dried beads) for 3 days (in a reciprocal shaker). Samples were collected and filtrated on 1 μm pore size filtration membrane and the filtrate was analyzed for residual Rb concentration using an inductively coupled plasma atomic emission spectrometer (ICP-AES, Jobin-Yvon Activa M). The pH was not controlled during the sorption but the final pH was recorded.

For sorption isotherms 50 mg of sorbent (m) were mixed with 20 mL (V) of Rb(I) solutions at different initial concentrations (C_0,

ranging between 10 and 500 mg Rb L^{-1}) for 3 days. The pH of the solutions was set at 3. After filtration, the residual concentration (C_{eq}, mg Rb L^{-1} or mmol Rb L^{-1}) was determined by ICP-AES and the sorption capacity (q, mg Rb g^{-1} or mmol Rb g^{-1}) was calculated by the mass balance equation: $q = (C_0 - C_{eq})\, V/m$.

For uptake kinetics 200 mg of sorbent were mixed with 500 mL of Rb(I) solutions (C_0: 20 mg Rb L^{-1}) at pH 3. Samples were collected at fixed times and the residual concentrations were determined by ICP-AES after filtration. Each sorbent was tested with dried beads (DB), wet beads (WB), freeze-dried beads (FB), large size dried beads (DBL) and large size wet beads (WBL).

Dynamic sorption tests were performed in fixed bed columns (internal diameter 7 mm) filled with 1 g of sorbent (Phozir and AMP, dried beads). The columns were fed upward at a flow rate of 42 mL h^{-1} (i.e., superficial flow velocity: 1.1 m h^{-1}). Rubidium concentration was 25 mg Rb L^{-1}. A fraction collector was used and the outlet concentration was measured by ICP-AES. A similar procedure was used for testing Rb(I) desorption using an ammonium nitrate/nitric acid solution (3 M NH_4NO_3/5 M HNO_3). The flow rate was decreased to 6 mL h^{-1} (i.e., superficial velocity: 0.2 m h^{-1}).

3. Results and discussion

3.1. Characterization of encapsulated sorbents

SEM and SEM–EDX analyses have been performed on the three materials (alginate capsules containing AMP, Phozir and the combination AMP + Phozir) before and after Rb(I) sorption. Figs. 1 and 2 show the morphology of cross-sections of AMP and Phozir encapsulated materials (Fig. AM1 shows the AMP + Phozir material, see Supplementary material). The cross-sections clearly demonstrate that the bulk materials are homogeneous (Figs. 1a, c and 2a, c). The sorption of Rb(I) does not change significantly the shape of the beads. The changes are more marked when comparing the aspect of encapsulated materials. While Phozir has a crystalline structure that appears in Fig. 1d as small micrometric spherical agglomerated particles enclosed in the cavities formed by the macromolecular network (large alveoli of several tens of microns), AMP-based material is characterized by the presence of much smaller, very dense and well-dispersed microparticles (Fig. 2d). This observation is consistent with those published by Mimura et al. [27], and Ye et al. [22].

Fig. 3 shows the energy-dispersive X-ray spectrum that identifies the major elements. The figure also shows the distribution of O, P, Ca and Zr through the cross-section of Phozir adsorbent: P and Zr elements are representative of the inorganic ion-exchanger, while Ca delineates the encapsulating material (calcium gelling of alginate). All these elements are homogeneously distributed. In addition the profile of phosphorus along the cross-section of the beads confirms that the sorbent microparticles of Phozir are homogeneously distributed within their organic matrix. Fig. 4 refers to Phozir-based material after Rb(I) sorption. Elemental mapping confirms the homogeneous distribution of both the inorganic ion exchange material and the sorbed metal. Further profiling along a cross-section displays a perfect correlation of Rb with P and Zr, thereby demonstrating that Rb is directly connected to the presence of Phozir. Similar observations were made for the AMP-based composite material both before (Fig. 5) and after (Fig.6) Rb(I) sorption. Homogeneous cross-sections are observed (O, Ca, P and Mo elements in Fig. 5; and P, Mo, Rb elements in Fig. 6). The profile of distributions are correlated for AMP (Mo and P elements, in the raw material) and for AMP + Rb (correlation between Mo and P elements on one side and Rb element on the other side). These results confirm the active role of AMP on Rb(I) binding. Similar conclusions can be reached, as expected, for the composite material made from a blend of Phozir and AMP (at the same dry weight proportion) (see Figs. AM2 and AM3).

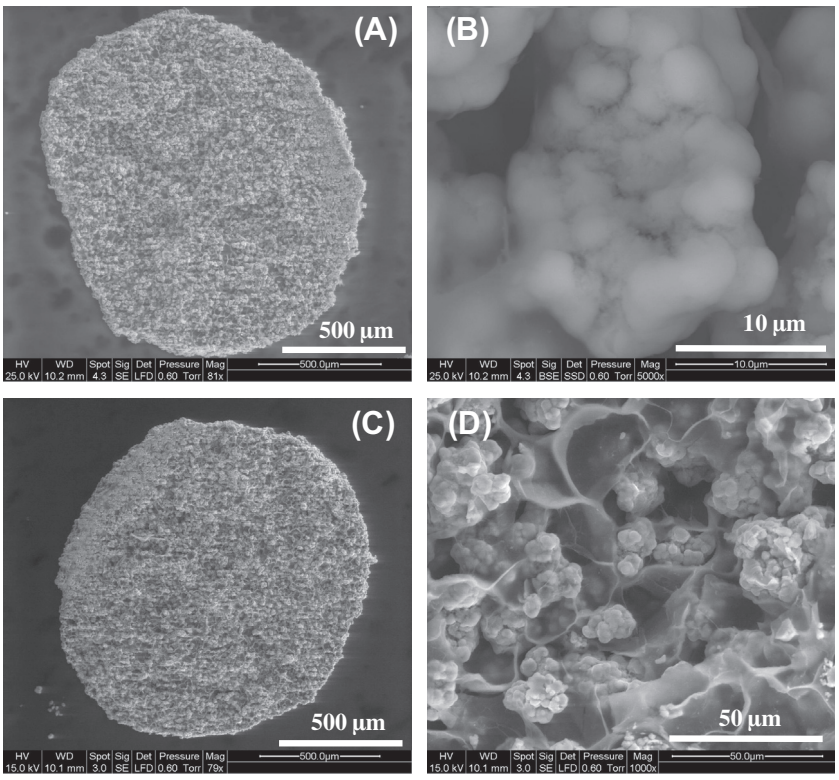

Fig. 1. SEM of Phozir immobilized in alginate capsules – morphology (A and B: raw material; C and D after Rb(I) sorption).

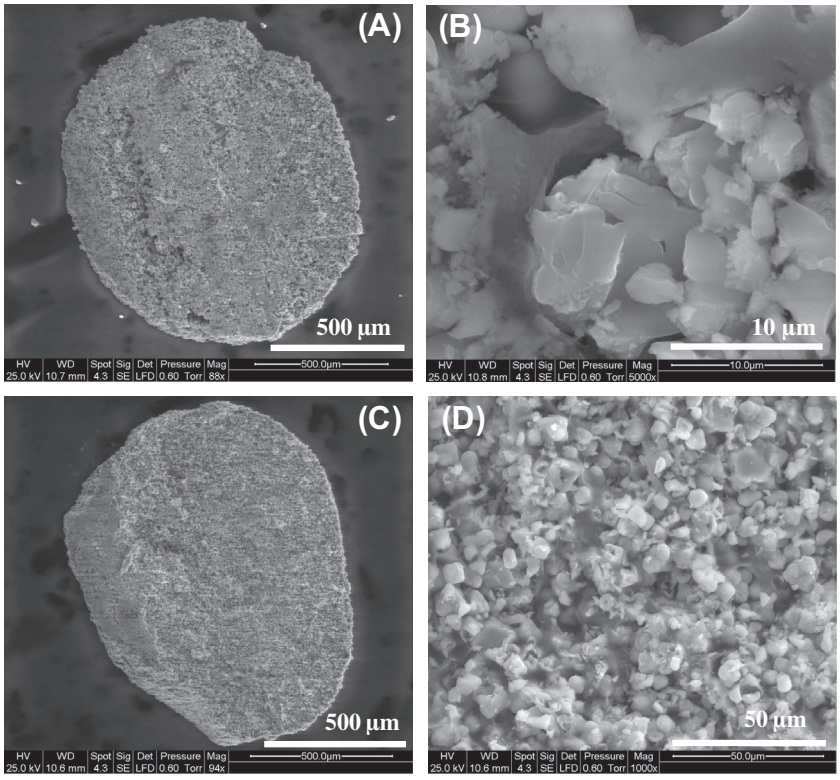

Fig. 2. SEM of AMP immobilized in alginate capsules – morphology (A and B: raw material; C and D after Rb(I) sorption).

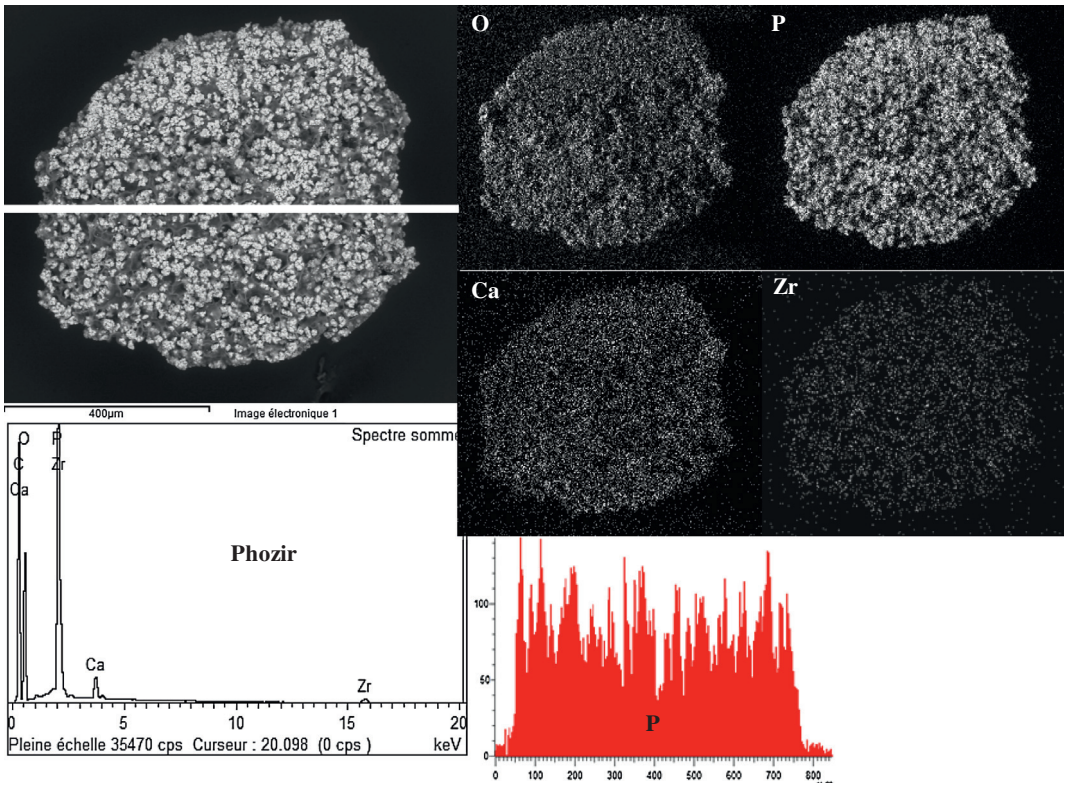

Fig. 3. SEM–EDX analysis of Phozir immobilized in alginate capsules: microphotograph of cross-section, X-ray diffraction pattern, element distribution, and cross-section distribution of elements.

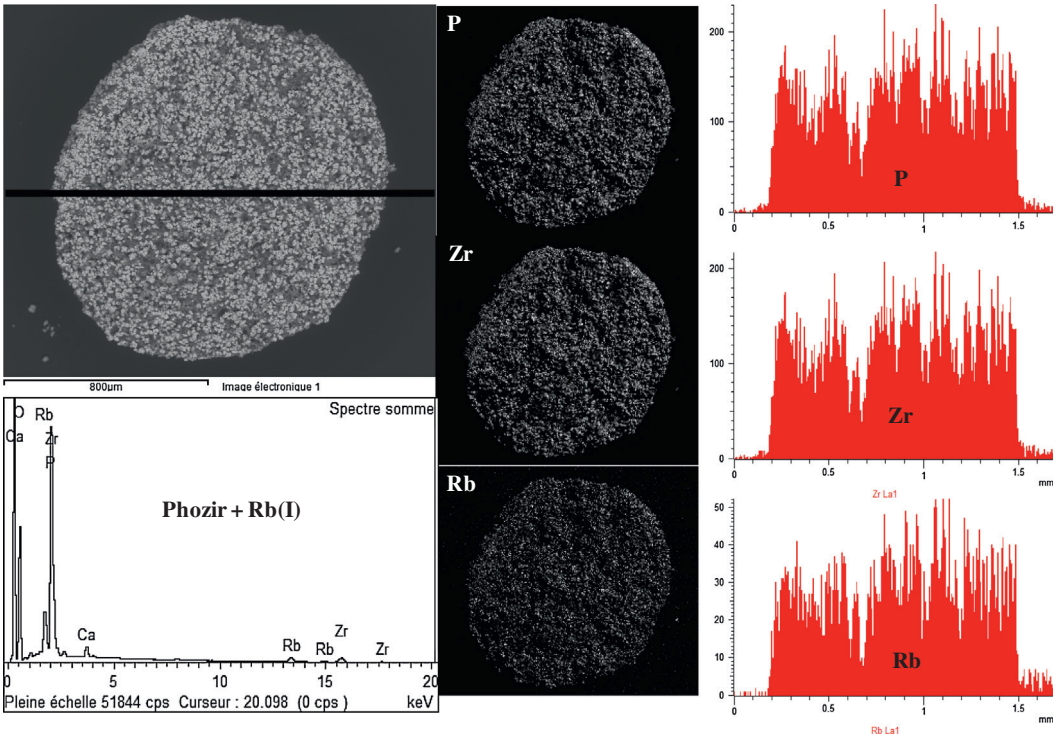

Fig. 4. SEM–EDX analysis of Phozir immobilized in alginate capsules after Rb(I) sorption: microphotograph of cross-section, X-ray diffraction pattern, element distribution, and cross-section distribution of elements.

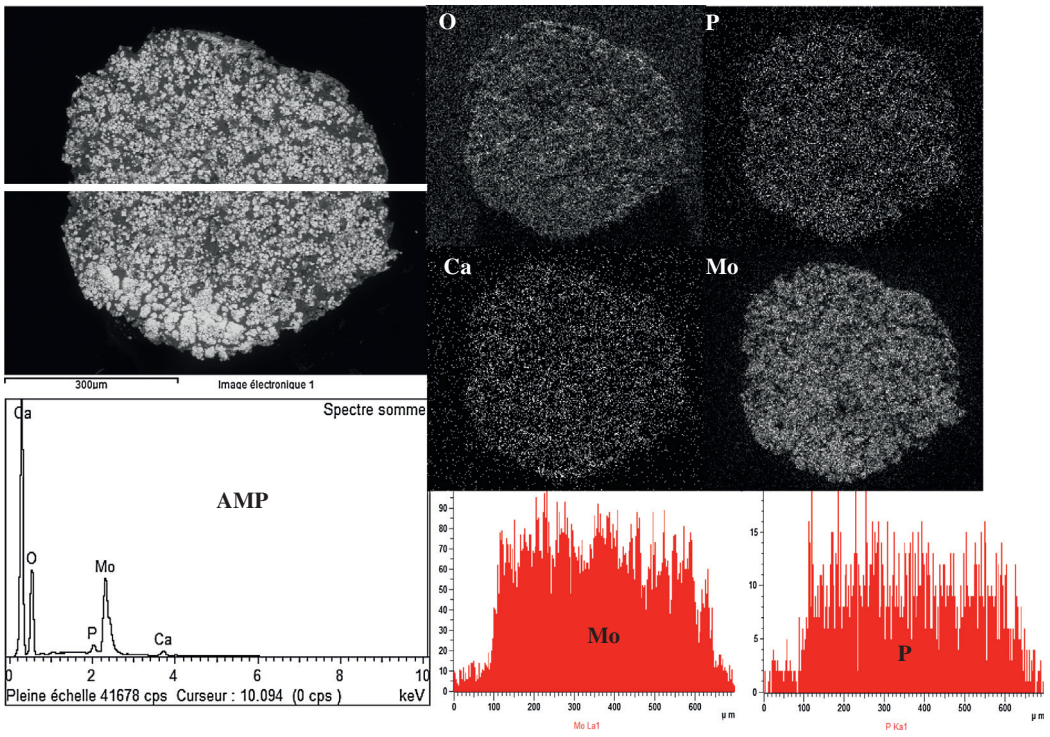

Fig. 5. SEM–EDX analysis of AMP immobilized in alginate capsules: microphotograph of cross-section, X-ray diffraction pattern, element distribution, and cross-section distribution of elements.

3.2. Effect of pH

Fig. 7a shows the effect of pH on Rb(I) sorption in the range of pH 1–6. The stability of the encapsulating material limits the possibility to use these encapsulated materials above pH 6. Under selected experimental conditions (i.e., C_0: 100 mg Rb L^{-1}; sorbent dosage (SD): 2.5 g L^{-1}) the sorption capacity reaches a maximum value close to 0.4 mmol Rb g^{-1} (i.e., 34 mg Rb g^{-1}). However, the behaviors of the different systems are significantly different: while AMP does not show significant differences in the range of pH 1–3,

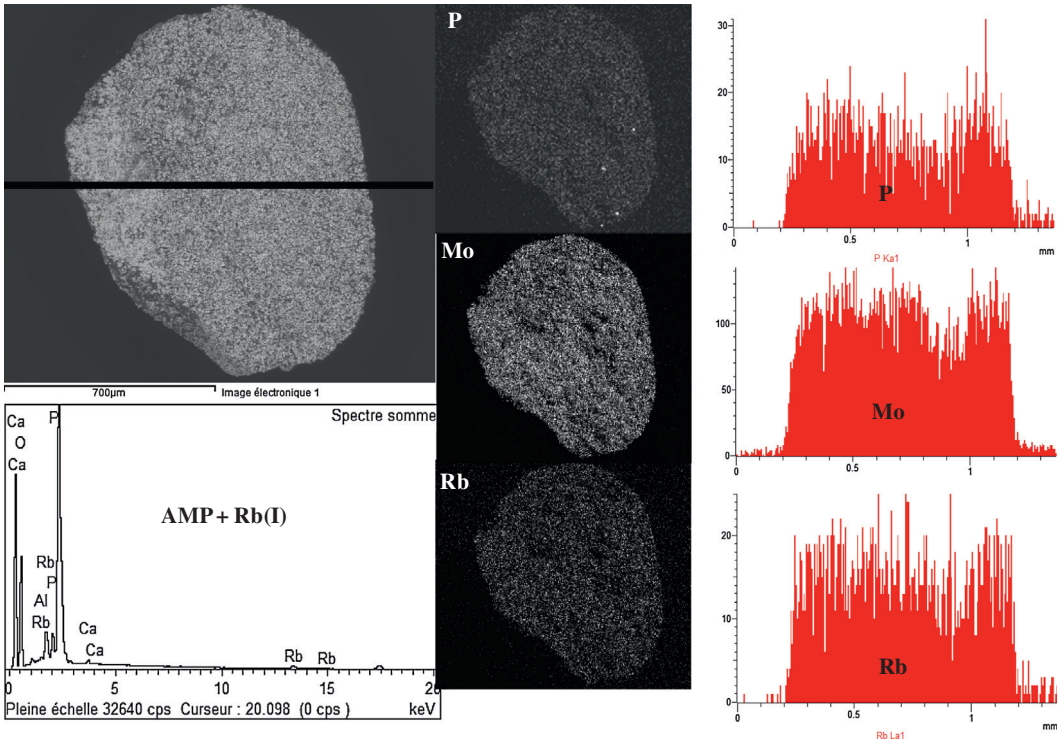

Fig. 6. SEM–EDX analysis of AMP immobilized in alginate capsules after Rb(I) sorption: microphotograph of cross-section, X-ray diffraction pattern, element distribution, and cross-section distribution of elements.

for Phozir the sorption capacity increases progressively with increasing the pH of the solution. In the case of the composite material made of equal amounts of AMP and Phozir, the behavior is intermediate between those of the individual inorganic ion exchangers. The second panel of the figure (Fig. 7b) shows the comparison between the initial and the final pH. In the range 1–3, the pH is hardly affected during metal sorption. Above pH 3, the equilibrium pH tended to reach a constant value in the range 2.7–3.4. The sorbent has a buffering effect, maintaining the pH close to 3 in low acidic solution (initial pH above 3.5) These pH variations and the buffering effect can be attributed to the exchange of protons on Phozir ($Zr(HPO_4)_2$). In the case of metal cation exchange with zirconium phosphate, Pan et al. [52] reported the stoichiometric exchange of protons with Pb(II), Cd(II) and Zn(II) that causes significant pH variations. When supporting zirconium phosphate on cation exchange resins, Pan et al. [45] also noticed a comparable effect of equilibrium pH on the sorption of Pb(II) with a progressive increase of metal sorption up to pH 3 followed by a stabilization of sorption efficiency. In the case of Phozir entrapped in polysulfone capsules Ma et al. [29] observed a continuous increase of the sorption efficiency with the initial pH (though they did not discuss the results as a function of the equilibrium pH).

$$Zr(HPO_4)_2 + Pb^{2+} \rightarrow ZrPb(PO_4)_2 + 2H^+ \quad (1a)$$

And by analogy with Cs [28]:

$$Zr(HPO_4)_2 + Rb^+ \rightarrow ZrRbH(PO_4)_2 + H^+ \quad (1b)$$

In the case of AMP the ion exchange process takes place between the target metal cation and ammonium ion making the pH variation less significant than that associated with the proton exchange occurring with Phozir. This may explain the minor pH change observed for AMP-based sorbents. By analogy with Park et al. [21]:

$$(NH_4)_3PMo_{12}O_{40} + n\,Rb^+ \rightarrow Rb_n(NH_4)_{3-n}PMo_{12}O_{40} + n\,(NH_4)^+ \quad (2)$$

Nilchi et al. [47] prepared AMP–polyacrylonitrile composites for Cs sorption and observed a limited effect of pH on the distribution coefficient. Chakravarty et al. [20] observed a more significant effect of pH on Cs distribution coefficient when using AMP impregnated on alumina microspheres.

3.3. Sorption isothrms

Rubidium distribution between the liquid and solid phases at equilibrium is described by the sorption isotherms obtained at pH 3 (Fig. 8). Despite a little dispersion of data between the series, the three sorbents have a very similar shape in terms of sorption isotherms. The sorption isotherms are characterized by a sharp initial increase of the sorption capacity followed by a stabilization at high Rb(I) residual concentration. This shape is characteristic of Langmuir-type isotherms (compared to the exponential form of Freundlich-type isotherms).

The isotherms have been modeled using the Langmuir equation:

$$q = (q_m \times b\,C_{eq})/(1 + b \times C_{eq}) \quad (3)$$

with q and q_m are the sorption capacities (mmol Rb g^{-1}) in equilibriumwith residual concentration C_{eq} (mmol Rb L^{-1}) and at saturation of the monolayer, respectively; b is the affinity coefficient (L $mmol^{-1}$). The parameters (i.e., q_m and b) of the Langmuir equation for the different systems are reported in Table 1. The parameter $q_m \times b$ (also reported in the table) is representative of the initial slope of the isotherm curves and is analogous to a distribution coefficient (L g^{-1}).

The maximum experimental sorption capacity is around 0.6 mmol Rb g^{-1} (i.e., 51 mg Rb g^{-1}) for AMP-based sorbent and reaches up to 0.7 mmol Rb g^{-1} (i.e., 60 mg Rb g^{-1}) for Phozir-based

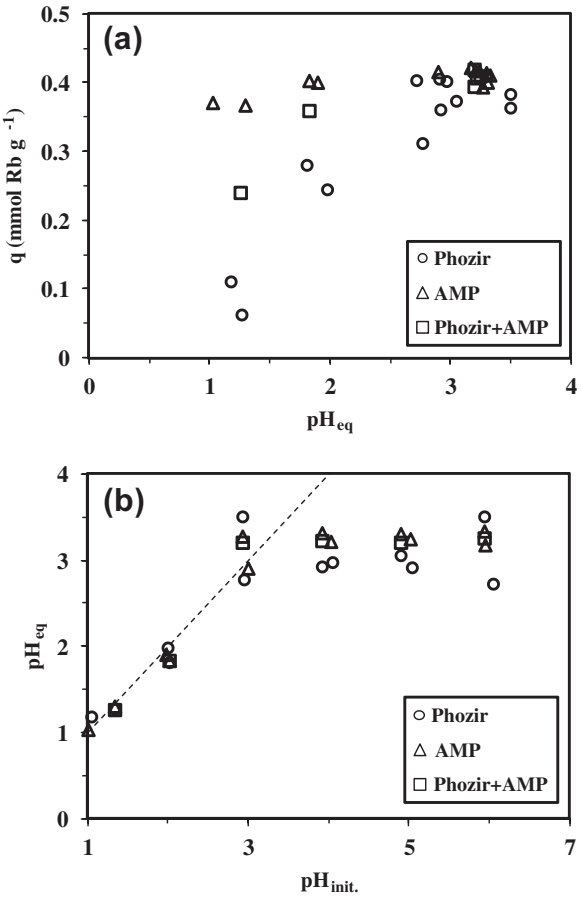

Fig. 7. Effect of pH on the sorption of Rb(I) (a) using Phozir, AMP and Phozir + AMP immobilized in alginate capsules and pH variation during Rb(I) sorption (b) (C_0: 100 mg Rb L^{-1}; m: 50 mg; V: 20 mL).

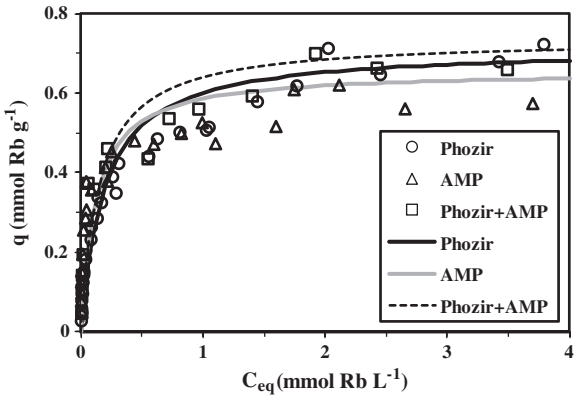

Fig. 8. Comparison of Rb(I) sorption isotherms for Phozir, AMP and Phozir + AMP encapsulated materials (pH 3; solid lines: modeling of isotherms with the Langmuir model, parameters in Table 1).

Table 1
Sorption isotherms – parameters of the Langmuir equation.

Sorbent	q_m (mmol Rb g^{-1})[a]	b (L $mmol^{-1}$)	$q_m \times b$ (L g^{-1})	R^2
Phozir	0.714 [61.1]	5.26	3.76	0.987
AMP	0.656 [56.1]	8.42	5.52	0.954
AMP + Phozir	0.735 [62.8]	6.64	4.88	0.984

[a] Number into brackets shows maximum sorption capacity in mg Rb g^{-1}.

sorbent (intermediate value for mixed AMP + Phozir material). Based on the solid content of the sorbents (inorganic ion-exchanger mass against total biopolymer + inorganic ion-exchanger total mass) close to 73%; the sorption capacities of these materials for Rb(I) are varying between 0.82 and 0.96 mmol Rb g^{-1} of inorganic ion-exchanger (i.e., 70 and 84 mg Rb g^{-1}). These values are of the same order of magnitude than those found in the literature for the binding of Rb(I) and Cs(I) on AMP–alginate composite (i.e., 0.55 mmol Rb g^{-1} and 0.65 mmol Cs g^{-1}, respectively) [22]. The amount of potentially exchangeable protons (for Phozir-based materials) is close to 3.8 mmol exch. g^{-1} while the amount of potentially exchangeable ammonium groups (for AMP-based materials) is close to 1.2 mmol exch. g^{-1}. This means that Phozir has about three times more exchangeable reactive groups than AMP in encapsulated materials while their effective maximum sorption capacities are broadly similar. In both cases the maximum sorption capacity is far below maximum exchangeable capacities, probably reflecting the fact that a significant fraction of these exchangeable groups are not available or accessible for interacting with Rb(I). Indeed, Banerjee et al. [23] compared raw AMP (free powder) and AMP-impregnated on resorcinol formaldehyde resins for the binding of cesium. They observed that the stoichiometric ratio at saturation of the AMP powder leads to the exchange of nearly two of the three ammonium ions present in AMP. This interpretation is also consistent with previous results on the ion exchange of Cs with AMP powder showing that 58% of exchangeable ammonium ions were exchanged at saturation [53]. The theoretical exchange capacity of AMP is 1.57 mmol eq. g^{-1}. Based on the weight content of AMP in the encapsulated material the theoretical exchange capacity of AMP-encapsulated material is close to 1.1 mmol eq. g^{-1}. The maximum sorption capacity is close to 0.6 mmol Rb g^{-1}; that is, means a sorption capacity close to 0.55 mmol Rb meq^{-1} (consistently with previous studies [23,53]). In the case of zirconium phosphate, Mrad et al. [28] compared three ion-exchangers synthesized with different procedures and characterized by different crystallinity. It was found that their weight exchange capacities varied between 6.3 and 8.9 mmol eq. per g, depending on the specific phase. Jiang et al. [54] compared Pb(II) sorption properties for two types of zirconium phosphate (amorphous and crystalline forms) and they observed that the weight exchange capacity strongly decreased with the increasing crystallinity of the ion-exchanger (1.5 versus 0.2 mmol eq. per g). These authors discussed the change in the sorption capacity with reference to both the size of cavities in the mineral phase and the hydrated/non-hydrated status of the metal ions. Pan et al. [52] investigated the binding of a series of divalent metal cations using amorphous zirconium phosphate. They established by potentiometric titration that the proton exchange capacity was closed to 6.1 mmol g^{-1} while the maximum amount of protons potentially released to the solution was close to 3 meq g^{-1}. The sorption capacity is close to 0.7 mmol Rb g^{-1}; this is far below the theoretical weight exchange capacity (in the range 6–9 mmol eq. g^{-1}). This discrepancy may be explained by (a) the formation of aggregates that decrease the accessibility to reactive groups and/or (b) the progressive decrease in the affinity of the sorbent for target metal ions (as a result of the change in the electronic environment of reactive groups when the sorbent progressively saturates). In any case there is a large excess of exchangeable sites compared to the amount of Rb(I) that could be adsorbed at saturation.

The affinity coefficients are of the same order of magnitude for the three sorbents (in the range 5.26–8.42 L $mmol^{-1}$); these values are slightly higher than those cited by Ye et al. [22] for Rb(I) (i.e., 1.65–3.06 L $mmol^{-1}$) and Cs(I) (i.e., 3.42–3.69 L $mmol^{-1}$) using AMP immobilized in alginate capsules. In the case of iron(III) hexacyanoferrate(II) immobilized on polymethylmethacrylate the

affinity coefficient was close to 2.1 L mmol^{-1} [18]. The term $q_m \times b$, analogous to a distribution coefficient, is varying between 3.76 and 5.52 L g^{-1} for the three sorbents.

3.4. Uptake kinetics

Uptake kinetics can be controlled by a series of different diffusion steps: (a) bulk diffusion (in the reactor volume), film (or external) diffusion, and intraparticle diffusion; apart of chemical reaction that may contribute to the control of mass transfer.

Changing the size of the particles, modifying the physical state of the particles with different modes of drying the composite beads offer various strategies that can be used for evaluating the contribution of the resistance to intraparticle diffusion on the control of uptake kinetics. Figs. 9–11 compare the kinetic profiles for the three sorbents for both large (L) and small beads (S under similar experimental conditions for materials that were used as produced (WB, wet beads), air-dried (DB, dried beads), freeze-dried (FB). Small beads reach the equilibrium within the first 2 h of contact while large beads require increasing the contact time to 4–6 h, under selected experimental conditions. This provides direct evidence that the resistance to intraparticle diffusion plays an important role in the control of mass transfer. Conversely, the comparison of small beads, either wet or dried using different methods shows that the type of drying does not affect the uptake kinetics. In many

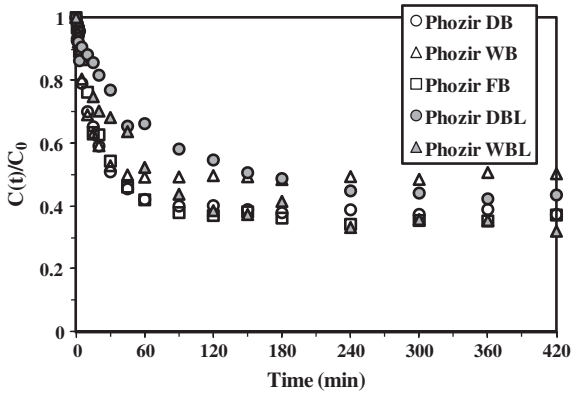

Fig. 9. Influence of material conditioning on Rb(I) uptake kinetics using Phozir immobilized in alginate capsules (pH 3; C_0: 20 mg Rb L^{-1}; SD: 400 mg sorbent L^{-1}; DB: dried beads, WB: wet beads, FB, freeze-dried beads, DBL: dried beads large size, WBL: wet beads large size).

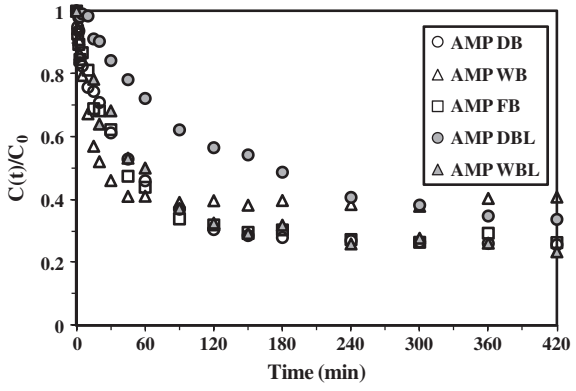

Fig. 10. Influence of material conditioning on Rb(I) uptake kinetics using AMP immobilized in alginate capsules (pH 3; C_0: 20 mg Rb L^{-1}; SD: 400 mg sorbent L^{-1}; DB: dried beads, WB: wet beads, FB, freeze-dried beads, DBL: dried beads large size, WBL: wet beads large size).

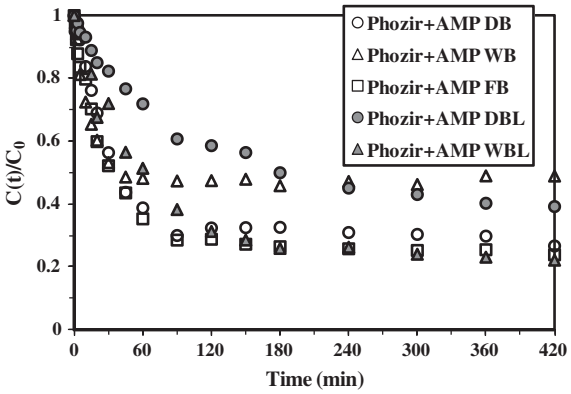

Fig. 11. Influence of material conditioning on Rb(I) uptake kinetics using Phozir + AMP immobilized in alginate capsules (pH 3; C_0: 20 mg Rb L^{-1}; SD: 400 mg sorbent L^{-1}; DB: dried beads, WB: wet beads, FB, freeze-dried beads, DBL: dried beads large size, WBL: wet beads large size).

cases, the freeze-drying technique allows minimizing the capillary forces that appear when drying biopolymer gels. This contributes to prevent or minimize the collapse of theinitial structure of the hydrogel. As a consequence the kinetics of sorption are generally faster when the hydrogel is freeze-dried and rehydrated than in the case of a hydrogel dried at room temperature (or in an oven) and subsequently rehydrated [55]. In the present case the freeze-drying does not significantly affect the kinetic profile of Rb(I) sorption, regardless of the type (or combination) of inorganic ion-exchanger that was immobilized in alginate capsule. Presumably, this can be probably explained by the presence of rigid inorganic particles that prevent the collapse of the structure and maintain (at least partially) the initial porous structure of the composite material. A similar effect was observed for chitosan hydrogel particles that were dried in the presence of sucrose: the gel beads were immersed in a concentrated solution of sucrose before being dried. After rehydration (and partial restoration of the initial size of the beads) the kinetic profiles that were obtained for the sorption of Pd(II) and Pt(IV) were intermediary between air-dried and freeze-dried materials [55]. The presence of sucrose crystallized during the drying step in the porous network contributed to prevent the collapse of the structure. Phozir and AMS, as rigid crystalline phases, are probably playing the same role in the present case. It is noteworthy that the profiles for the wet materials are superimposed to the other sorbents in the initial section of the curves (within the first hour of contact) while the second section tends to level off faster than for the others and equilibrates within 60 min of contact but at a residual concentration that was slightly higher than the levels reached with dried beads and freeze-dried beads. The slightly less favorable behavior of wet beads in terms of equilibrium performance may be attributed to the difficulty to achieve a constant mass of sorbent: with dried materials the accurate weighing of the beads is much easier than in the case of wet materials that contain variable water content (within and at the surface of the materials). A slight overestimation of the amount of sorbent effectively dropped into the solution may cause the slight shift towards higher equilibrium concentration. The faster contact time for equilibrium confirms that the resistance to intraparticle diffusion has a non-negligible effect on mass transfer but the presence of solid particles in the biopolymer network allows maintaining high mass transfer properties and minimizing the collapse of the structure when drying (irrespective of the method used for that purpose).

The intraparticle diffusion coefficient (D_e, effective diffusivity, m^2 min^{-1}) was determined using Crank's equation, assuming the

solid to be initially free of metal, and the kinetics to be controlled by intraparticle diffusion resistance [56]:

$$\frac{q(t)}{q_{eq}} = 1 - \sum_{n=1}^{\infty} \frac{6\alpha(\alpha+1)\exp\left(\frac{-D_e q_n^2 t}{r^2}\right)}{9 + 9\alpha + q_n^2\alpha^2} \quad (4)$$

$q(t)$ and q_{eq} are the concentrations of the metal in the resin at time and equilibrium, respectively, r is the radius of the particle and q_n non-zero roots of the equation:

$$\tan q_n = \frac{3q_n}{3 + \alpha q_n^2} \quad (5)$$

The equation was applied for determining the diffusion coefficient for all kinetic data using the software package Mathematica®. An example of data fitting is shown in Section 2.1 (Fig. AM4). Table 2 reports the values of the intraparticle diffusion coefficients based on the results of Figs. 9–11. As expected the intraparticle diffusion coefficient increases with wet material (in the range 17.5×10^{-10}–26.1×10^{-10} m^2 min^{-1}) while for air-dried and freeze-dried beads the values are roughly the same (in the range 2.4×10^{-10}–8.2×10^{-10} m^2 min^{-1}). On the other hand for coarse beads (L) the intraparticle diffusivity coefficients are significantly decreased (by a factor of ca. 2) for wet materials. For air-dried materials the intraparticle diffusion coefficients are roughly the same for small and coarse beads, whatever the inorganic ion-exchanger immobilized in alginate capsules.

3.5. Dynamic studies: breakthrough curves and desorption profiles

The breakthrough curves were obtained for Phozir and AMP based materials (Fig. 12). Both Phozir and AMP profiles are characterized by (a) a first step where Rb(I) was completely removed by the sorbent, (b) a breakthrough occurring after 4 and 9 h for Phozir and AMP, respectively (i.e., approximately 200 and 500 BVs, bed-volumes), (c) a progressive increase of the outlet concentration (almost linear for AMP and curved for Phozir-based materials), and (d) the saturation of the sorbent occurring at about 54 h (i.e., around 3000 BVs for AMP and around 200 BVs for Phozir). The mass balance equation (comparing initial metal concentration and metal concentration in the collector of waste solutions) leads to estimates of Rb(I) binding close to 22 mg for Phozir-based and close to 36 mg for AMP-based materials. These values can be compared with those deduced from the sorption isotherms; specifically, for a residual concentration of 25 mg Rb L^{-1} (i.e., 0.3 mmol Rb L^{-1}) the sorption capacities should be close to 37 and 40 mg Rb g^{-1} for Phozir and AMP, respectively (i.e., 0.44 and 0.47 mmol Rb g^{-1} for Phozir and AMP, respectively). Therefore,

Table 2
Intraparticle diffusion coefficient (Crank's equation) – modeling of uptake kinetics.

Sorbent	Intraparticle diffusion coefficient $D_{eff} \times 10^{10}$ (m^2 min^{-1})	Mean square of residuals (MSR)
Phozir DB	8.21	0.038
Phozir WB	26.1	0.028
Phozir FB	4.78	0.023
Phozir DBL	7.31	0.048
Phozir WBL	14.6	0.022
AMP DB	2.40	0.026
AMP WB	19.0	0.024
AMP FB	2.60	0.032
AMP DBL	2.97	0.042
AMP WBL	8.45	0.023
Phozir + AMP DB	3.32	0.073
Phozir + AMP WB	17.5	0.054
Phozir + AMP FB	3.73	0.023
Phozir + AMP DBL	4.29	0.020
Phozir + AMP WBL	8.40	0.032

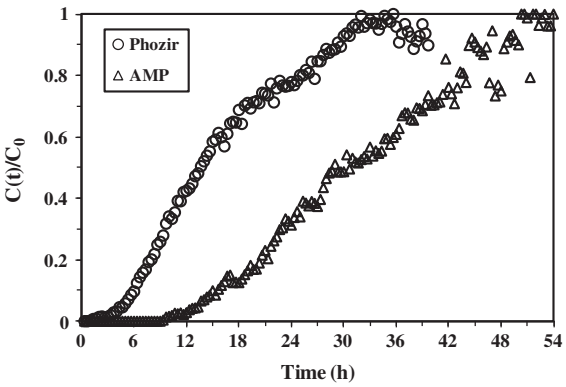

Fig. 12. Breakthrough curves for the sorption of Rb(I) using Phozir and AMP immobilized in alginate capsules (dried beads; pH 3; C_0: 20 mg L^{-1}; amount of sorbent: 1 g; flow rate: mL h^{-1}).

the sorption capacity is in agreement with theoretical predictions for AMP-based material but significantly lower for Phozir-based materials.

The studies in batch reactors have shown kinetic profiles that were much closer between Phozir and AMP-based materials than the breakthrough curves obtained in the dynamic mode. Specifically, AMP-based sorbent shows a much greater efficiency than those based on Phozir, e.g., delayed breakthrough and saturation times. The saturation of thesorbent would require installing 5–6 columns in series for AMP and about 8–10 columns in series for Phozir-based sorbent (in order to achieve both the complete recovery of Rb(I) and the saturation of the sorbent in the first column; full use of the column and total metal recovery).

Metal desorption can be operated using ammonium chloride (or nitrate) as shown by Nilchi et al. [47] for Cs(I) sorption and desorption using AMP immobilized in polyacrylonitrile beads. Ammonium chloride was also cited as a good eluent for AMP–silica gel (prepared by the sol–gel method) sorbents [57]. For cesium desorption from potassium copper–nickel hexacyanoferrate(II) sorbent, Ishfaq et al. [58] showed that nitric acid can be efficiently used. For desorption of uranium from zirconium phosphate sorbent, Borovinskii et al. [59] suggested using 2 M nitric acid solutions. In the case of alginate–AMP composite Mimura et al. [48] proposed using a mixture of ammonium chloride and nitric acid for the elution of Cs(I) from loaded particles. Specifically, nitric acid was used in an attempt to prevent the excessive swelling of the biopolymer beads during the desorption step. For our experiments we also used a mixture of ammonium chloride and nitric acid (Fig. 13). Metal desorption was quite efficient in terms of concen-

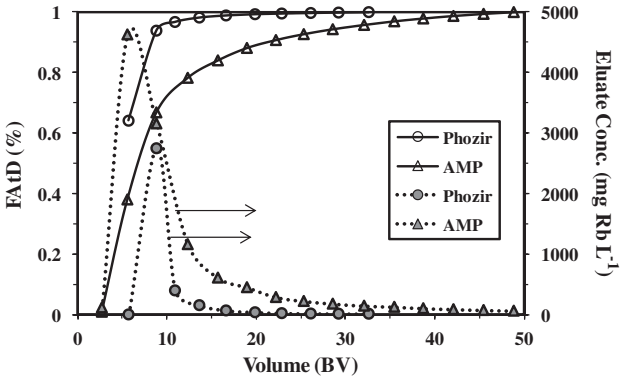

Fig. 13. Rb(I) desorption of Phozir and AMP based materials in dynamic mode.

tration effect. More than 95% of the total stripping occurred within the first 10 BVs for Phozir-based sorbent and peak concentration was over 3 g Rb L^{-1}. The mass balance applied to the desorption step showed that more than 95% of the metal that was initially bound was desorbed from the column. In the case of AMP sorbent the results are slightly less attractive: total removal reached 70% after 50 BVs, the peak concentration reached almost 5 g L^{-1} but the desorption profile is characterized by a long tail that demonstrates that a fraction of Rb(I) remained in the sorbent and required larger volumes of eluent.

4. Conclusion

Ammonium molybdophosphate and zirconium phosphate ion-exchangers can be efficiently embedded in alginate capsules for preparing Rb(I) sorbents. The combination of AMP and Phozir in the same encapsulate does not change significantly their sorption behavior. SEM and SEM–EDX analyses show that (a) the inorganic ion-exchangers are homogeneously distributed in the capsules and (b) the metal can also be bound homogeneously in the whole volume of the sorbent. The metal can be sorbed at pH 3: AMP-based sorbent being less sensitive to pH than Phozir-based counterpart. The sorption isotherms are described by the Langmuir equation and the maximum sorption capacity varies between 0.65 and 0.74 mmol Rb g^{-1} (i.e., 56–63 mg Rb g^{-1}). Uptake kinetics is controlled by the intraparticle diffusion as shown by the effect of particle size. Compared to the dramatic loss of porosity that may occur in dried alginate beads, the presence of inorganic rigid particles in the biopolymer capsules limits the adverse effects of the drying process, by preventing the collapse of the porous network. The freeze-drying procedure does not improve the mass transfer properties: the solid particles contribute to preventing the collapse of the porous structure during the drying step. As a consequence, the kinetic profiles (and the intraparticle diffusion coefficients) are not impacted by the drying method; though the intraparticle diffusion coefficients are significantly higher for wet beads (against dried materials). Breakthrough curves confirm the interest of these granular composites for the recovery of Rb(I) in dynamic systems: higher efficiency of AMP- versus Phozir-based sorbent. Ammonium chloride combined with nitric acid allows desorbing Rb(I) from loaded sorbents: the desorption was easier for Phozir (complete) than for AMP (partial; i.e., 70%). Complementary investigations are necessary for evaluating the life cycle of the sorbents and optimizing the desorption step. These materials could be used for analytical processes (selective pre-concentration) or for recovery of radionuclides (applications currently under investigation).

Acknowledgments

Région Languedoc-Roussillon is acknowledged for the regional fellowship attributed to P.K.

Authors acknowledge the technical contribution of Julien Abbe, Geoffrey Leibundgut and Robin Kurtz.

References

[1] V.N. Epov, D. Lariviere, K.M. Reiber, R.D. Evans, R.J. Cornett, J. Anal. At. Spectrom. 19 (2004) 1225.
[2] B.S. Mohite, S.H. Burungale, Anal. Lett. 32 (1999) 173.
[3] M. Shamsipur, K. Alizadeh, M. Hosseini, M.F. Mousavi, Anal. Lett. 38 (2005) 573.
[4] M. Burgard, L. Jurdy, H.S. Park, R. Heimburger, New J. Chem. 7 (1983) 575.
[5] N.M. Hassan, W.D. King, D.J. McCabe, L.L. Hamm, M.E. Johnson, J. Radioanal. Nucl. Chem. 253 (2002) 361.
[6] R. Ratner, L. Kogan, D.H. Kohn, J. Chromatogr. 148 (1978) 539.
[7] S.I. Kargov, L.A. Shelkovnikova, V.A. Ivanov, Russ. J. Phys. Chem. 86 (2012) 860.
[8] Y. Onodera, H. Mimura, T. Iwasaki, H. Hayashi, T. Ebina, M. Chatterjee, Sep. Sci. Technol. 34 (1999) 2347.
[9] T. Sasaki, S. Tanaka, Chem. Lett. 41 (2012) 32.
[10] B. Hu, B. Fugetsu, H. Yu, Y. Abe, J. Hazard. Mater. 217–218 (2012) 85.
[11] P.J. Faustino, Y. Yang, J.J. Progar, C.R. Brownell, N. Sadrieh, J.C. May, E. Leutzinger, D.A. Place, E.P. Duffy, F. Houn, S.A. Loewke, V.J. Mecozzi, C.D. Ellison, M.A. Khan, A.S. Hussain, R.C. Lyon, J. Pharm. Biomed. Anal. 47 (2008) 114.
[12] B. Le Gall, F. Taran, D. Renault, J.C. Wilk, E. Ansoborlo, Biochimie 88 (2006) 1837.
[13] C.-Y. Chang, L.-K. Chau, W.-P. Hu, C.-Y. Wang, J.-H. Liao, Microporous Mesoporous Mater. 109 (2008) 505.
[14] T.A. Denisova, L.G. Maksimova, O.N. Leonidova, M.A. Melkozerova, N.A. Zhuravlev, E.V. Polyakov, Russ. J. Inorg. Chem. 54 (2009) 649.
[15] S. Taj, M. Ashraf Chaudhry, M. Mazhar, J. Radioanal. Nucl. Chem. 281 (2009) 393.
[16] V. Epimakhov, L. Moskvin, V. Chetverikov, T. Epimakhov, A. Ganyushkin, S. Prokhorkin, Radiochemistry 52 (2010) 610.
[17] M. Mostafa, M.A. El-Absy, M. Amin, M.A. El-Amir, A.B. Farag, J. Radioanal. Nucl. Chem. 285 (2011) 579.
[18] S. Taj, D. Muhammad, M.A. Chaudhry, M. Mazhar, J. Radioanal. Nucl. Chem. 288 (2011) 79.
[19] Ľ. Vrtoch, M. Pipíška, M. Horník, J. Augustín, J. Lesný, J. Radioanal. Nucl. Chem. 287 (2011) 853.
[20] R. Chakravarty, R. Ram, K.T. Pillai, Y. Pamale, R.V. Kamat, A. Dash, J. Chromatogr. A 1220 (2012) 82.
[21] Y. Park, Y.C. Lee, W.S. Shin, S.J. Choi, Chem. Eng. J. 162 (2010) 685.
[22] X.S. Ye, Z.J. Wu, W. Li, H.N. Liu, Q. Li, B.J. Qing, M. Guo, F. Go, Colloids Surf. A 342 (2009) 76.
[23] D. Banerjee, M.A. Rao, J. Gabriel, S.K. Samanta, Desalination 232 (2008) 172.
[24] T.J. Tranter, R.S. Herbst, T.A. Todd, A.L. Olson, H.B. Eldredge, Adv. Environ. Res. 6 (2002) 107.
[25] T.A. Todd, N.R. Mann, T.J. Tranter, F. Sebesta, J. John, A. Motl, J. Radioanal. Nucl. Chem. 254 (2002) 47.
[26] H. Mimura, Y. Onodera, J. Nucl. Sci. Technol. 39 (2002) 282.
[27] H. Mimura, M. Saito, K. Akiba, Y. Onodera, J. Nucl. Sci. Technol. 38 (2001) 872.
[28] O. Mrad, A. Abdul-Hadi, H. Arsan, J. Radioanal. Nucl. Chem. 287 (2011) 177.
[29] X. Ma, Y. Li, X. Li, L. Yang, X. Wang, J. Hazard. Mater. 188 (2011) 296.
[30] R. Thakkar, U. Chudasama, J. Hazard. Mater. 172 (2009) 129.
[31] M.G. Almazan-Torres, R. Drot, F. Mercier-Bion, H. Catalette, C. Den Auwer, E. Simoni, J. Colloid Interface Sci. 323 (2008) 42.
[32] B. Pan, B. Pan, X. Chen, W. Zhang, X. Zhang, Q. Zhang, Q. Zhang, J. Chen, Water Res. 40 (2006) 2938.
[33] F. Bauer, M. Willert-Porada, Solid State Ionics 177 (2006) 2391.
[34] S.I. Borovkov, L.M. Sharygin, Russ. J. Appl. Chem. 78 (2005) 229.
[35] K.M. Parida, B.B. Sahu, D.P. Das, J. Colloid Interface Sci. 270 (2004) 436.
[36] V.N. Lebedev, N.A. Mel'nik, A.V. Rudenko, Radiochemistry 45 (2003) 149.
[37] D. Zhao, F.F. Li, A.Y. Zhang, L. Yang, R. Zhu, Acta Crystallogr. C 67 (2011) I4.
[38] R. Chourasia, A. Bohre, R.D. Ambastha, O.P. Shrivastava, P.K. Wattal, J. Mater. Sci. 45 (2010) 533.
[39] V. Sydorchuk, S. Khalameida, J. Skubiszewska-Zięba, R. Leboda, J. Therm. Anal. Calorim. 103 (2011) 257.
[40] T. Sangvanich, V. Sukwarotwat, R.J. Wiacek, R.M. Grudzien, G.E. Fryxell, R.S. Addleman, C. Timchalk, W. Yantasee, J. Hazard. Mater. 182 (2010) 225.
[41] P.N. Pathak, G.R. Choppin, J. Radioanal. Nucl. Chem. 270 (2006) 299.
[42] S. Van Le, L. Szirtes, J. Radioanal. Nucl. Chem. 99 (1986) 45.
[43] J. Satyanarayana, G.S. Murthy, P. Sasidhar, J. Radioanal. Nucl. Chem. 242 (1999) 11.
[44] Q. Zhang, P. Jiang, B. Pan, W. Zhang, L. Lv, Ind. Eng. Chem. Res. 48 (2009) 4495.
[45] B.C. Pan, Q.R. Zhang, W.M. Zhang, B.J. Pan, W. Du, L. Lv, Q.J. Zhang, Z.W. Xu, Q.X. Zhang, J. Colloid Interface Sci. 310 (2007) 99.
[46] T.J. Tranter, R.S. Herbst, T.A. Todd, Adsorption 8 (2002) 291.
[47] A. Nilchi, R. Saberi, M. Moradi, H. Azizpour, R. Zarghami, J. Radioanal. Nucl. Chem. 292 (2012) 609.
[48] H. Mimura, W. Yan, Y. Wang, Y. Niibori, I. Yamagishi, M. Ozawa, T. Ohnishi, S. Koyama, Nucl. Eng. Des. 241 (2011) 4750.
[49] P. Agulhon, M. Robitzer, L. David, F. Quignard, Biomacromolecules 13 (2012) 215.
[50] H. Mimura, H. Ohta, K. Akiba, Y. Onodera, J. Nucl. Sci. Technol. 38 (2001) 342.
[51] E. Guibal, T. Vincent, C. Jouannin, J. Mater. Chem. 19 (2009) 8515.
[52] B. Pan, Q. Zhang, W. Du, W. Zhang, B. Pan, Q. Zhang, Z. Xu, Q. Zhang, Water Res. 41 (2007) 3103.
[53] I. Cunha, L. Sakai, J. Radioanal. Nucl. Chem. 131 (1989) 105.
[54] P. Jiang, B. Pan, B. Pan, W. Zhang, Q. Zhang, Colloids Surf. A 322 (2008) 108.
[55] M. Ruiz, A. Sastre, E. Guibal, Sep. Sci. Technol. 37 (2002) 2143.
[56] J. Crank, The Mathematics of Diffusion, second ed., Oxford University Press, Oxford, G.B., 1975.
[57] J. Doležal, J. Stejskal, M. Tympl, V. Kouřím, J. Radioanal. Nucl. Chem. 21 (1974) 381.
[58] M.M. Ishfaq, H.M.A. Karim, M.A. Khan, J. Radioanal. Nucl. Chem. 170 (1993) 321.
[59] V.A. Borovinskii, E.V. Lyzlova, L.M. Ramazanov, Radiochemistry 43 (2001) 84.